although variation of the maximum zero-voltage current with inductance was seen. The presence or absence of hysteresis is thus presumed to be an indicator of the capacitive/inductive nature of the device.

These two cases are extremes in the sense that constant voltage of constant current sources are employed. In an experimental situation, one has only a voltage source with a series resistance. The effect of a realistic source on the I-V curves has been studied (Warman and Blackburn 1971, 1972) and the results may be summarized as follows: For an inductive system, the main effect is to produce a negative resistance region, which extends to some voltage determined by the inductance and the ratio $\beta = R_s/R_j$ (source resistance and Josephson device resistance). Beyond this voltage, the current increases with increasing voltage, finally merging with the $\beta = 0$ characteristic.

For a capacitive system with large-source resistance, the features noted by Stewart are observed. In particular, hysteresis caused by the appearance of a rotational branch is seen. As β is decreased, a negative resistance region develops and, at the same time, the rotational branch is displaced upward to higher currents. Below a certain β_{min}, this rotational solution vanishes and a single reversible I-V characteristic results. We wish to emphasize that, in this regime, the inductive and capacitive models are qualitatively indistinguishable; and that assignment of L or C by curve fitting to experimental data could be misleading.

The negative resistance region implied by our results has been experimentally observed (Buckner *et al.* 1970; Shapiro 1963).

II. WEAK LINKS AS RADIATION DETECTORS

a) *Effect of an Electromagnetic Field on Weak Links.*

As we mentioned before, Eq. (3) implies that a D.C. voltage V_0 applied across a weak link generates an A.C. component of frequency,

$$\omega_0 = 2e\,V_0/\hbar.$$

the frequency $2e/\hbar$ is rather high (483.6 MHz/μV). If, by means of electromagnetic radiation, we induce an additional A.C. voltage of frequency ω_1, Eq. (3) becomes

$$\frac{d\Phi}{dt} = \frac{2e}{\hbar}(V_0 + V_1 \cos \omega_1 t) \qquad (7)$$

or, integrating,

$$\Phi(t) = \frac{2e}{\hbar}\left(V_0 t + \frac{1}{\omega_1}\sin\omega_1 t\right) + \Phi_0. \qquad (8)$$

Substituting Eq. (8) in (2), taking $\Phi_0 = 2\pi$ (which corresponds to the maximum zero voltage current) and using the standard relations

$$\cos(x\sin\alpha) = \sum_{n=-\infty}^{\infty} J_n(x)\cos(n\alpha)$$

$$\sin(x\sin\alpha) = \sum_{n=-\infty}^{\infty} J_n(x)\sin(n\alpha),$$

where J_n are Bessel functions of order n,

$$I(t) = I_0 \sum_{n=-\infty}^{\infty} J_n\left(\frac{2eV_1}{\hbar\omega_1}\right)\cos(\omega_0 + n\omega_1)\,t. \qquad (9)$$

That is, for voltages such that $\omega_0 + n\omega_1 = 0$, there is a D.C. contribution to the current (voltage steps),

$$I_{DC} = I_0 (-1)^n J_n\left(\frac{2eV_1}{\hbar\omega_1}\right) \qquad (10)$$

at fixed voltages, which correspond to the harmonics of ω_1.

If, instead, we induce across the link two A.C. voltages at frequencies ω_1 and ω_2, a similar derivation gives, instead of Eq. (9),

$$I = I_0 \sum_{n=-\infty}^{\infty}\sum_{m=-\infty}^{\infty} J_n\left(\frac{2eV_1}{\hbar\omega_2}\right) J_m\left(\frac{2eV_2}{\hbar\omega_2}\right)$$

$$\sin[\omega_0 t + \Phi_0 + n(\omega_1 t + \phi_1) + m(\omega_2 t + \phi_2)] \qquad (11)$$

where Φ_0, Φ_1, Φ_2 are constants and, instead of Eq. (10), we get as an expression for the maximum zero voltage current,

$$I_{DC} = I_0 J_0\left(\frac{2eV_1}{\hbar\omega_1}\right) J_0\left(\frac{2eV_2}{\hbar\omega_2}\right) \qquad (12)$$

where we have chosen $\Phi_0 = \pi/2$. Eq. (11) not only implies the occurrence of steps at the harmonie frequencies of ω_1 and ω_2, but, also, at the mixed frequencies $\omega_1 \pm \omega_2$.

b) *Current and Voltage Bias*

In an experimental situation, one has the choice to operate the weak link from a voltage or from a current source. This is equivalent to a choice of $\beta = 0$ (perfect voltage source) or $\beta >> 1$ (in the limit $\beta \to \infty$ one has a perfect current source). From a practical point of view, it is easier to make a current source (a battery in series with a variable resistor will be enough). Due to the low impedance of a typical weak link ($\sim .1\Omega$), in order to have a true voltage source, one has to have a very low source impedance. Nevertheless, this is certainly possible (Blackford 1971).

However, the radiation induced structure of the I-V characteristic will not be identical for the two cases. The results shown in Eqs. (9) to (11) assume implicitly that one is using a voltage source. That is, we take a given expression for the voltage. We introduce it in Eq. (3), (see Eq. 7). We solve for Φ (t), and we use this Φ to obtain, through Eq. (2), an expression for the current flowing in the circuit. Eq. (9) shows that this method gives constant voltage steps at the harmonic frequencies

$$\omega_0 = n\omega_1.$$

Let us say that we use a D.C. current source, and we represent the incoming radiation by an A.C. current supply, in series with the bias source. Kirchhoff's law for this circuit is

$$I_0 + I_1 \cos\omega_1 t = I_0 \sin\Phi + \frac{2e}{\hbar}\sigma\frac{d\Phi}{dt}, \qquad (13)$$

where this time we take the current as given, and we want to find $<\frac{d\Phi}{dt}>$, the average voltage. One has to use numerical methods to solve this equation; but the results show (Waldram *et al.* 1970) constant voltage steps at both the harmonic *and* subharmonic frequencies of ω_1; *i. e.*, when

$$m\omega_0 = n\omega_1.$$

The subharmonic structure was first observed in weak links (point-contacts or bridges as opposed to tunnel junctions). This has been generally assumed to come from microscopic short circuits across the insulating layer, or from the presence of an inductive reactance in the weak link (see Figure 2). However, the fact that Eq. (13) does not contain an inductive term and yet predicts the subharmonic structure is very puzzling for the author. One possible explanation is that subharmonic structure would appear in Eq. (9), if the Josephson current-phase relation Eq. (2) would not be sinusoidal. By the same token, one can raise the question of how fair is it to represent the incoming radiation by a voltage source (Eq. 7) and not by a current source (Eq. 13).

c) *Broad Band Detection*

Clearly, the zero voltage current represents a n = 0 step for any frequency of the incident radia-

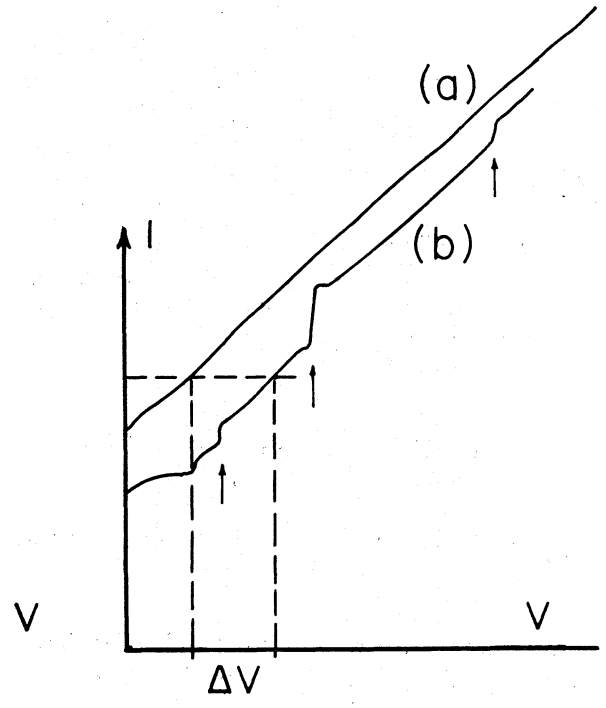

FIG. 2. A weak link load curve with (b) and without applied radiation(a). Both harmonic and subharmonic structures are manifest.

tion. Hence, by monitoring its height, one operates the weak link as a broadband detector. If we take Eq. (10) for n = 0 and in the limit of small signals, we get

$$\delta I_0 = -\frac{1}{4} I_0 \left(\frac{2e}{\hbar\omega_1}\right) \delta V_1^2, \qquad (14)$$

where δI_0 is the change in critical current due to δV_1. That is, we get a square law detector (in units of voltage) or a linear response detector (in units of power). A convenient experimental arrangement consists of current biasing the link slightly above the critical current I_0 and modulating the amplitude of the incoming radiation (*e.g.* with a chopper). Then, one can use a phase sensitive lock-in amplifier to detect the change in voltage, due to the change in the value of I_0 (ΔV in Figure 2).

d) *Heterodyne Detection*

Of course, one can apply the same biasing scheme to other harmonic steps. We can interpret the voltage steps as zero frequency beats between the A.C. Josephson current and the nth harmonic of the incident radiation. Then, by monitoring the height of the steps, we obtain a heterodyne detector that uses the A.C. Josephson current as a local oscillator. Eq. (10) gives, in the limit of small V_1,

$$I_{DC} = \frac{I_0}{n!} \left(\frac{eV_1}{\hbar\omega_1}\right)^n; \qquad (15)$$

therefore, monitoring the n = 1 step we get a linear detector, the n = 2 step a square law detector, and so on. However, the scheme of biasing that is convenient for the n = 0 step has some serious drawbacks for the harmonic steps. The most important is its inconvenience for the measurement of small signals, since in order to bias in the region of high differential resistance (that would yield high sensitivity) one needs a finite step height. In the limit of small incident power, only the n = 0 step has a finite height.

There are two different ways to overcome this difficulty. The first one is to locate the weak link in a resonant cavity. The theory of the Josephson effect has been extended to include this case (Grimes *et al.* 1968). Essentially, what happens is that the cavity is driven by the Josephson A.C. current and, in its turn, it induces steps on the I-V characteristic of the junction at the voltage corresponding to the resonant frequency. One overcomes the above mentioned problem and it is possible to monitor the height of the *cavity induced step,* in the presence of incoming radiation. A heterodyne detector is thus obtained that uses the cavity as a local oscillator (Richards and Sterling 1969).

Finally, the weak link can be operated as a mixer, as suggested by Eqs. (11) and (12). If in Eq. (11) ω_1 is taken very close to ω_2, $\omega_1 - \omega_2$ can be an intermediate frequency (e.g. 30MHz). Very low noise amplifiers are available at these frequencies and can be used to detect the I-F radiation coming from the step at $\omega_1 - \omega_2$.

e) *The Impedance Matching Problem*

Every geometry of weak coupled superconductors, that has manifested Josephson-like behavior, has a common feature. The resistance in the I-V characteristic is of the order of 0.1Ω. If we want to use the weak link as a detector in the microwave or infrared regions, this impedance has to be matched to that of a waveguide or light pipe, which is typically of the order of 370Ω. If the incident power on the waveguide is P_0, the voltage it generates on the weak link (V_1 on Eq. 7) will be, in general, given by

$$V_1 = \left[4 \frac{Z_1^2 Z_0}{(Z_1 + Z_0)^2} P_0\right]^{1/2}, \qquad (16)$$

where Z_0, Z_1 are the impedances of the link and the waveguide, respectively. If we use a perfect matching transformer, $Z_1 = Z_0$ and Eq. (16) reduces to

$$V_1^2 = Z_1 P_0. \qquad (17)$$

Therefore, even for perfect matching, high junction impedances are desirable. However, the noise due to phase slippage is proportional to the resistance of the weak link. Both factors should be kept in mind.

f) *General Features of a Josephson Detector*

i) *Frequency Response.* The response of a Josephson detector is limited on the low-frequency

limit by the smallness of the voltage that one is able to detect that is, since

$$2e/\hbar \simeq 484\ \mathrm{MHz}/\mu\mathrm{V},$$

frequencies of the order of 500 KHz will induce steps at $v \sim 1$ nV. Experiments have been reported (Kamper and Zimmerman 1971) which use a few KHz. For high frequency, the response is limited by the energy gap. That is, when the frequency ω of the radiation is such that

$$\hbar\omega \sim \Delta g \sim 1{\cdot}5 - 2 \cdot kT_c,$$

where T_c is the critical temperature of the superconductor, it will induce only quasiparticle tunneling. The higher the frequency the more the behavior of the superconductor will resemble that of a normal metal. However, the energy gap is not a sharp boundary and high sensitivities have been reported for frequencies as high as $4\Delta g$ (Grimes *et al.* 1968). Clearly, a weak link made up of Nb_3Sn ($T_c \sim 18°K$), will extend its range to twice of one made of Pb ($T_c \sim 9°K$). Only in this respect (and obvious mechanical properties) will the particular material influence the behavior of a weak link. This range of applicability extends into the far infrared (wavelengths of the order of 100-200 μ).

ii) *Noise.* Several treatments of noise can be found in the literature for diverse geometries in Josephson junctions (Stephen 1969). We shall only sketch some of the more relevant results. The first one concerns the noise introduced in the junction by an external measuring circuit at room temperature. The way this problem has been treated is by adding to the Josephson device circuit equation a fluctuating noise current (white noise) term that has an average value $2kR^{-1}T$. The main effect related to the introduction of this term is a change in the value of the maximum zero voltage current; hence in the height of all the constant voltage steps. As the fluctuations increase, the zero voltage supercurrent is reduced and a supercurrent maximum appears at a *non-zero voltage*. This, in effect, amounts to a rounding of the super-normal transition. Figure 3 shows this rounding-off as a function of the noise (Ambegaokar and Halperin 1969). Further increase in the noise leads to a further reduction of the

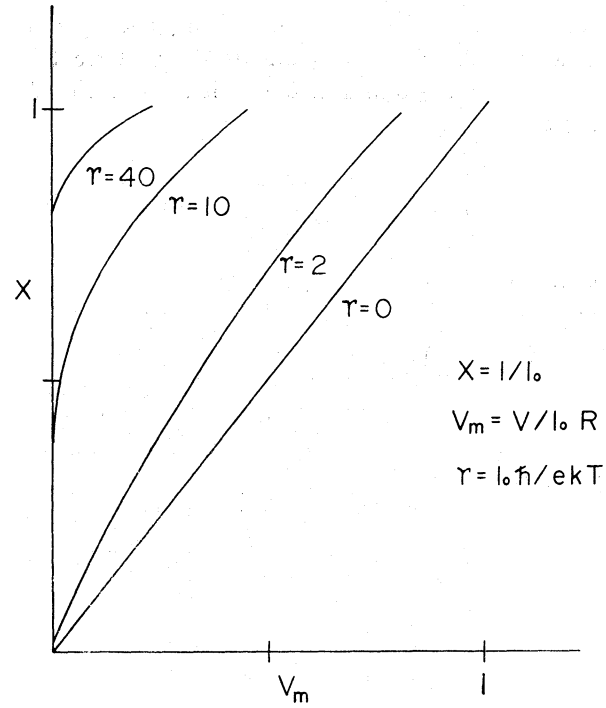

FIG. 3. Effect of noise in the I-V characteristics. Decreasing values of γ correspond to increasing noise.

maximum and to an increase of the voltage at which it appears. In the hight noise limit, the supercurrent is given by (Ivanchenko and Zil'berman 1969)

$$\left(\frac{I}{I_0}\right)_{dc} = \frac{z}{2}\,\frac{2eVD/\hbar}{(2eV/\hbar)^2 + D^2},$$

where I_0 is the supercurrent in the absence of noise, $D = kT_nR\,(2e\hbar)^2$, $z = \hbar I_0/2ekT_n$ (the ratio of the Josephson coupling energy to kT_n) and T_n is the effective noise temperature of the noise source. A different type of noise (shot noise) comes from random fluctuations in the junction when its temperature is low, $kT << eV$. This shot noise is equivalent to thermal noise at a certain effective temperature

$$T_{eff} \approx eV/k,$$

or using Josephson relation (3)

$$T_{eff} \approx \hbar\omega/2k$$

If one is working with $\omega \sim 20$GHz, then $T_{eff} \sim .5$°K. We must remark, however, that in most experimental situations these sources of noise are not necessarily dominant. Imperfections in the sample, which are very hard to avoid, have a very strong effect. A typical example is the fact that not all the link undergoes simultaneously the super-normal transition. This effect is particularly noticeable in the powder junction and causes noise through the redistribution of supercurrents and a rapid change in the value of the resistance. Other effects, such as: trapped flux, radiation pickup, pickup noise through the line, and temperature variations in the bath (bubbling in the LHe) also affect strongly the limiting noise.

iii) *Sensitivity and Speed.* The sensitivity performance of the Josephson detectors is rather good. Typical figures for the Noise Equivalent Power are 10^{-13} W/$\sqrt{\text{Hz}}$ on the broad-band mode (coupled through a cavity) and 10^{-14} W/$\sqrt{\text{Hz}}$ for the regenerative detector in the IR region. This compares favorably with other existing IR detectors; *e. g.*, the germanium bolometer. The theoretical relaxation time for a Josephson detector is $\sim 10^{-12}$ sec. and its speed of response has been measured to be faster than 10ns (Grimes *et al.* 1968). This response time means that variations that have very short periods, like those in pulsars (typical period $\sim .3$ sec), can be measured.

III. TYPES OF JOSEPHSON DEVICES

There is a large diversity of geometries that exhibit the Josephson effects. In this section, we discuss some of the most common of these.

a) *Cross-wire junction*

This junction is made by pressing together two superconducting wires (usually Nb, due to its mechanical strength) that have been heat-treated to produce a layer of oxide on their surface. This oxide layer acts as the insulator between superconductors. In practice, however, the oxide layer is not perfect and the presence of micro-shorts between the superconductors causes a weak link behavior in this type of device, rather than a true junction. It presents serious drawbacks to its practical use as a detector. First: although it is relatively simple to fabricate, on recycling it changes its characteristics very drastically, due to differential contraction in the metal and insulator holder that keeps a constant pressure on the wires. Second: it is very difficult to couple radiation to the sensitive area; hence yielding a large N.E.P. The best N.E.P. we were able to obtain using this type of weak link was of the order of 10^{-12} watt $\sqrt{\text{Hz}}$.

b) *Solder-blob junction*

This type is, again, very simple to fabricate. One only has to deposit a drop of standard Sn/Pb solder on a heat-treated superconducting wire (Nb). At low temperatures, the solder is also a superconductor and the oxide layer on the wire acts as an insulator. The blob-type weak link is very stable, has excellent recycling properties, and is very sensitive to changes in biasing current or voltage (Clarke 1970). As such, it has been successfully used in building superconducting galvanometers (SLUG). However, from the point of view of a radiation detector, it presents a very serious problem. Radiation cannot penetrate the solder drop and reach the sensitive junction. The only possible scheme to couple the weak link to radiation is via an inductive coupling of the superconducting wire, i.e., letting it act as an antenna. To our knowledge, this coupling scheme has not been fully explored.

c) *Tunnel or SIS junction*

This type of junction is made by depositing two thin film strips, approximately 1 mm. wide and 1000 Å thick, on a substrate forming a cross, and oxidizing the first one. Therefore in the overlapping region of the two strips, one has a Superconductor-Insulator-Superconductor sandwich. This device exhibits true Josephson junction behaviour. However, the S-I-S sandwich has a large capacitance, thus presenting a large reactive mismatch at large frequencies and reflecting most of the incident radiation. One way to overcome this problem is to make the thin film strips much narrower (v.g. 20 microns). The capacitance depends on the area of the sandwich; hence on the square of the factor by

which we reduce the width of the film strips. The technical problems involved in making such narrow film strips have been overcome (McCarthy and Warman 1974) via electron-beam fabrication techniques. However, there remains to be tested the sensitivity and recycling properties of these narrow tunnel junctions.

d) *Powder junction*

This type of junction has been extensively studied by the author and the results have been reported (Warman 1972; Warman, Jahn and Kao 1971). The device is made by pressing together a large number (10000) of superconductiong small grains (av. diam. ~ 45 microns). The resulting detector can be highly sensitive; in fact, we have obtained N.E.P.'s as low a 10^{-14}W/$\sqrt{\text{Hz}}$. However, from the point of view of a practical detector, their reliability is poor. A more reliable detector, based on the same principle, has been extensively studied by T.D. Clark (1968). Yet, the properties of this type of junction are quite complex and their practical application remains to be studied.

e) *Point-Contact junction*

This junction is made by pressing a pointed superconducting wire (the point is made by filing or etching) against a flat superconducting surface. Typical materials are Nb-Sn, Ta-Sn, and Pb-Sn or Pb-Pb. The only detector system that has been applied to Astronomy makes use of this type of weak link (Ulrich 1974). The detector has been successfully used in observing at 1 mm and 2 mm wavelengths at McDonald Observatory. Although the I-V characteristics remain constant only up to 10% through recycling, nightly calibration can overcome this problem. Sensitivities of point contact devices range in the 10^{-13} W/$\sqrt{\text{Hz}}$ N.E.P. range. A complete description of the detector system can be found in the above-mentioned reference.

f) *Superconducting bridges*

Another geometry of interest, from the point of view of a radiation detector, is a superconducting bridge; *i.e.*, a small and narrow thin film, connecting two "bulk" superconductors (usually two large films). Phase correlation of the two bulk superconductors takes place through the bridge. An obvious attractive feature of this geometry is its mechanical stability, since once the film is deposited, it requires no further mechanical contact. Also, this geometry allows the preparation of clean samples, whose dimensions can be controlled. Finally, from the point of view of coupling to electromagnetic radiation, the bridge offers an "open" geometry; i.e., the sensitive area of the device is not surrounded by superconducting material. This should improve the efficiency of the coupling.

The first experiments with superconducting bridges in an electromagnetic field were reported by Dayem and Anderson (Dayem and Anderson 1964). Their bridges were deposited using a mask and were $\sim$4X2 μm in size. With applied radiation, they observed the presence of both harmonic and subharmonic steps, but the behavior of the bridge was not "Josephson-like" except very near the critical temperature.

In these bridges, sensitivity to radiation was rather poor. More recent work indicates (Warman 1972) that the range of temperatures in which the bridge shows Josephson behavior, could be extended by making smaller bridges.

To understand this behavior, it is convenient to reconsider briefly the basic Josephson relations. These are

$$I = I_0 \sin \Phi \qquad (2)$$

and

$$\Delta\mu = \hbar\dot{\Phi} \qquad (18)$$

$\Delta\mu$ being the change in chemical potential across the weak link. Clearly, taking $\Delta\mu = 2eV$ reduces the equation to its previous form. However, the point is that these equations are fundamentally different. Eq. (18) is valid for any chemical potential change in a superconductor, and is derived only from symmetry considerations on the complex order parameter, while Eq. (2) determines whether the superconductor shows Josephson behavior. (In order to avoid confusion, due to semantics, we specify "pure" Josephson behavior as the situation in which the current-phase Equation (2) is stricly satisfied). The dependence of the current-phase relation on the length of the bridge (more precisely, on the ratio of the length of the bridge and the coherence

length) has been studied theoretically by Baratoff *et al.* (1970), and independently by Christiansen *et al.* (1971). Baratoff takes a one-dimensional superconducting wire in which a section of length L has a smaller critical current. The solutions of the one-dimensional Ginzburg-Landau equations on this region, are found and fitted continuously (together with the derivatives) to the solutions in the rest of the wire. From these solutions, the current-phase relation can be obtained for the "weak" superconducting region. The results indicate that the current-phase relation is sinusoidal only when $L/\xi \ll 1$, and as L increases (or ξ decreases) the I-Φ curve becomes skew towards higher values of the argument. In the limit of very large L, even the periodic nature of I (Φ) is lost. Similar results were obtained by Christiansen, through a very different argument. He solved the one-dimensional Ginzburg-Landau equations for a small link connecting two large superconductors (using rigid boundary conditions at the end of the link), and redefined the phase as

$$\delta = \Phi + \alpha L_M, \tag{19}$$

where Φ is the usual phase, δ the redefined phase, L_M the self-inductance of the link, and α a parameter that depends on the temperature through the coherence length. For temperatures near T_c, the L_M contribution is negligible and one recuperates the sinusoidal I-Φ relation. However, when the coherence length becomes smaller, L_M contribution becomes important and, again, the I-Φ curve becomes skewed toward higher values of Φ. An attractive feature of the Christiansen model is that it allows for a difference in the critical temperature of the weak link and that of the bulk superconductors; while Baratoff's model assumes the same critical temperature for the link and the bulk.

The first experimental study of the current-phase relation was made by Fulton and Dynes (1970) and confirms the departure from the sinusoidal form as the temperature departs from T_c. A more recent study, made by Song (1972) on the effect of the ratio L/ξ on the behavior of a weak link, confirms the fact that near T_c ($L/\xi \ll 1$) the link shows Josephson behavior; while at low temperatures ($L/\xi \gg 1$), the link behaves as a "bulk" superconductor.

In the presence of an r-f field, the superconducting bridges manifest a unique behavior. This is an enhancement of the zero voltage current. Instead of following the Bessel function behavior under an increasing r-f field, the zero voltage current increases first. The effect was first studied by Dayem and Wiegand in 1964. Its importance for detection is evident, since (in the broadband mode) it is the behavior in the presence of small amounts of incident radiation that controls the response of the detector.

A probable explanation of the microwave enhancement of the critical current is due to Eliashberg (1970) and is based on the idea that, under certain conditions, an r-f field shifts the "center of gravity" of the excitations distribution function towards larger values of the energy, thereby increasing the ordering parameter Δ, through the equation

$$\Delta = g \int_{\Delta}^{\hbar\omega_D} d\varepsilon \frac{\Delta}{\sqrt{\varepsilon^2 - \Delta^2}} (1-2n(\varepsilon)), \tag{20}$$

where in equilibrium $n(\varepsilon) = 1/(1 + \exp(\varepsilon/T))$. More explicitly, for the case of a thin film in the dirty limit, Eq. (20) can be taken to the form

$$(\alpha - \beta^2\Delta^2 - \gamma - \delta\psi)\Delta = 0, \tag{21}$$

where

$$\begin{aligned} \alpha &= 1 - T/T_c \\ \beta^2 &= \frac{7\,\xi(3)}{8(\pi T_c)^2} \\ \gamma &= \frac{\pi}{6T_c}\frac{l v e^2}{hc^2}A_0^2 \\ \delta &= \frac{\pi}{6T_c}\frac{l v e^2}{hc^2}\frac{A_\omega^2}{2}. \end{aligned} \tag{22}$$

Where T_c is the critical temperature, A_0 takes into account the effect of static magnetic field and currents, and A_ω that of alternating fields. Also,

$$\Psi = 1 - \frac{\hbar\omega}{2\pi\eta} f\left(\frac{\hbar\omega}{\Delta}\right) \tag{23}$$

$$\eta = \hbar/\tau_0,$$

where τ_0 is the lifetime of the excitations, and f is a complicated function, whose asymptotic behavior is given by

$$f(u) = u \ln (8/u), u \ll 1,$$
$$f(u) = \pi/u, u \gg 1: \quad (24)$$

We notice first that for microwave radiation, $\hbar\omega/\Delta \ll 1$, so

$$f\left(\frac{\hbar\omega}{\Delta}\right) = \frac{\hbar\omega}{\Delta} \ln \frac{8\Delta}{\hbar\omega} \quad (25)$$

substituting (25) in (23),

$$\psi = 1 - \frac{h^2\omega^2}{2\pi\gamma\Delta} \ln \frac{8\Delta}{\hbar\omega} \quad (26)$$

Two facts become apparent from this equation:
i) There exists a critical frequency, ω_c, such that

$$\omega_c^2 \ln \frac{8\Delta}{\hbar\omega} = \frac{2\pi}{\hbar^2}\gamma\Delta$$

for frequencies under ω_c, $\psi > 0$ while if $\omega > \omega_c$, $\psi < 0$. ii) $\psi(\Delta)$ approaches rapidly its asymptotic value and there exists a wide range of Δ values for which $\psi(\Delta)$ is essentially independent of Δ. In this region, Eq. (21) can be solved as a quadratic equation whose positive root is given by

$$\Delta = \frac{1}{\beta}(\alpha - \gamma - \delta\psi)^{1/2} \quad (27)$$

From this equation, one can make some qualitative predictions. i) An r−f field of frequency $\omega > \omega_c$ will induce an increase in Δ; hence in the maximum zero voltage current. ii) A magnetic field depresses the value of Δ, yet, for each magnetic field, the enhancement of the critical current takes place. iii) For a given intensity of the r − f field, the increase in Δ will be larger for higher frequencies. Clearly, the frequencies cannot be too high or approximation (25) breaks down. This frequency effect has been observed by Dayem (1967). iv) The presence of an r−f field will enhance the critical temperature. Such an effect was studied by Wyatt and Evans (1969), although it was interpreted as due to some type of unspecified fluctuations.

IV. EXPERIMENTAL SET UP

Whatever the type of weak link being used, the experimental set-up is basically the same. The system we describe in the following paragraphs, is the one employed by the author in the study of three types of junctions; crossed wires, powder, and micro-bridges. Figure 4 shows the schematics of the physical set-up for laboratory tests. The basic parameters that control the behaviour of the junction are the temperature, magnetic field, and incident radiation. Hence, we immerse the junction in a LHe bath, in such a way that it is located in the center of an homogeneous magnetic field, and we provide a light pipe (or wave guide) system, with a chopper, to guide the incident radiation.

Figure 5 shows a block diagram of the measuring circuit. A voltage source S, in series with the variable resistor P (0 to 50 kΩ), acts as a current source

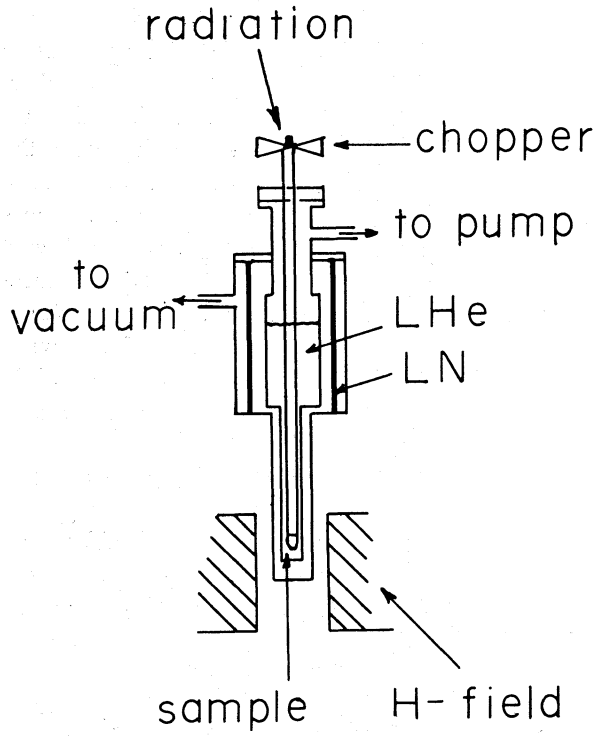

FIG. 4. Schematic diagram of the cryogenic system.

for the junction. The current is measured in the I channel by the voltage across R. Having R = 100Ω insures that the circuit acts as a current source for any value of P. The junction is considered a four terminal device and the V channel uses a differential input to measure the voltage across the junction. For testing, a function generator is used in place of S and is operated at any convenient frequency (~500 Hz). The I and V channels are the Y and X inputs (differential) of a Dual Beam Oscilloscope. In order to obtain I−V curves, the function generator can be operated in the sawtooth mode at a very low frequency (.1Hz). I − channel is then the Y imput of a X−Y recorder, while voltage is measured by a D.C. microvoltmeter, whose output goes to the X channel of the recorder.

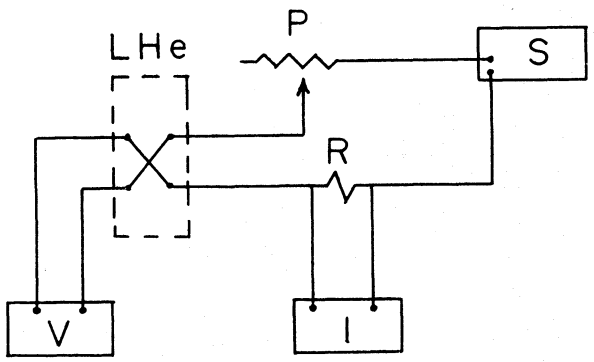

FIG. 5. Block diagram of the measuring system. Junction is shown as a four terminal device.

The sensitivity measurements are carried out with a D.C. voltage source as a bias. Radiation is amplitude-modulated and the voltage across the junction measured with the lock-in amplifier operating at the modulation frequency. A convenient value for this frequency was ~1 KHz. Usually, input impedances of the lock-in amplifier are high(10MΩ), while the impedance of the junction is quite small (typically .1 Ω). Hence, a matching transformer provides a first stage of amplification between the junction and the amplifier. The exact gain of these transformers depends on the impedance across their primary windings. Rather than determine this value for each bias current and compute the exact gain, we prefer to consider, for the purposes of sensitivity, junction and transformer as one unit and to compute the responsivity of the detector as the ratio of the voltage read at the lock-in and the power input.

The radiation detection tests in our experiments were carried out, almost without exception, in the microwave range. This was due to the availability of microwave equipment and the relative difficulty of obtaining infrared test equipment. An r−f generator, together with a frequency doubler, provided a versatile microwave source, covering the frequency ranges from 8.2 to 12.4 KMHz and from 16.4 to 24.8 KMHz. Attenuators allowed us to vary the power incident on the junction from 10^{-4} to 10^{-15} W.

a) *Calibration*

We have mentioned the fact that, in principle, a weak link has a very wide frequency response range. In practice, however, one must choose a frequency range of operation which is much narrower. In the broadband mode, this is equivalent to using filters. That is, the use of a given size waveguide (or light pipe) determines a range of operation, the same as it can transmit with minimum loss. A narrower range can be obtained by coupling into a cavity (Ulrich 1974). One must take into account all these coupling factors in the determination of an intrinsic N.E.P. figure.

Calibration can be made in several ways. One can compute the absolute amount of energy being sent into the waveguide by knowing the temperature of the emitting source (assuming it to be a black-body) and the spectral response of the detector system. Measuring then the response to that amount of energy gives a calibration directly in energy units. Alternatively, one can use as sources of radiation two black-bodies at known temperatures, and by measuring the relative response, get a calibration in temperature units. This last method is widely used in radioastronomy.

b) *Microbridges*

Our samples were prepared by the method suggested by Gregers-Hansen *et al.* (1971). A glass substrate is cleaned ultrasonically and washed in distilled water, acetone, and methanol. A first scratch is then made with a razor blade (tungsten stainless steel edge seems to give best results). A film of tin

is evaporated on the substrate, with a thickness of $\sim$1000 Å. A second scratch, perpendicular to the first, is made to remove all the tin except the one deposited in the furrow made by the first cut, constituting the bridge. By this method, one can obtain bridges of good quality and approximately $.5 \times 1\ \mu$m in size. However, the method has three severe drawbacks: i) The yield of good bridges is very low, $\sim$2%. ii) One cannot decide the size of the bridge prior to its fabrication. iii) The shape of the bridge is only approximately known. Furthermore, the edges of the bridge are not well defined and the debris left by the blade makes them uneven. This feature is important because the current density will be larger at the edges. If they are irregular, they will form a superconductor "weaker" than the bridge, thus the properties of the bridge will be really determined by those of the edges.

Figure 2 shows the I−V characteristic of one of our samples and the effect of incident microwave radiation. We note the presence of both harmonic and subharmonic series.

From the point of view of sensitivity, the entire theory applies without change to the narrow-band modes, and the theoretical estimates of ultimate sensitivity are the same. For the broadband mode, a theoretical estimate cannot be made without a better understanding of the Dayem effect. We have obtained experimentally sensitivities $\sim 10^{-12}\ \mathrm{W}\sqrt{\mathrm{Hz}}$. An improvement of this number depends on the possibility of fabricating cleaner and smaller samples. The need of these cleaner samples is also evident if one is to understand more clearly the Dayem Effect. With this motivation, we endeavored to improve the method of fabrication of microbridges. We have now been able to overcome most of the technical difficulties involved in making small, clean, and reproducible bridges by making use of electron-beam techniques. These techniques were first developed by the IBM group (Broers and Hatzakis 1970) and were adapted to the fabrication of small microbridges (McCarthy and Warman 1974). Now we have open several interesting possibilities: first, of course, the fabrication of microbridges in a reproducible manner, with their possible application to detection once a better understanding of the Dayem effect is achieved. Second, the possibility of making the narrow crossfilm tunnel junction. Third, the possibility of making narrow overlay-microbridges (Notary's bridges) of a previously unachieved size. This program is now being advanced.

REFERENCES

Ambegaokar, V. and Halperin, B. I. 1969, *Phys. Rev. Lett.*, **22**, 1364.

Anderson, P. W. and Dayem, A. H. 1964, *Phys. Rev. Lett.*, **13**, 195.

Baratoff, A., Blackburn, J. A. and Schwartz, B. B. 1970, *Phys. Rev. Lett.*, **25**, 1096.

Blackburn, J. A. and Warman, J. 1972, *App. Phys. Lett.*, **20**, 459.

Blackford, B. L. 1971, *Rev. Sci. Inst.*, **42**, 1198.

Broers, A. N. and Hatzakis, M. 1970, *Microscop. Electron.*, **1**, 249.

Buckner, S. A., Chan, J. T. and Langenberg, D. N. 1970, *Phys. Rev. Lett.*, **25**, 738.

Christiansen, P. V., Hansen, E. B. and Sjostrom, C. J. 1971, *J. Low Temp. Phys.*, **4**, 349.

Clark, T. D. 1968, *Phys. Lett.*, **27A**, 585.

Clarke, J. 1970, *Rev. de Physique App.*, **5**, 32.

Dayem, A. H. and Wiegand, J. J. 1967, *Phys. Rev.*, **155**, 419.

Eliashberg, G. M. 1970, *ZETP Fis. Red.*, **11**, 186.

Fulton, T. A. and Dynes, R. C. 1970, *Phys. Rev. Lett.*, **25**, 794.

Ginzburg, V. L. and Landau, L. D. 1950, *Zh. Eksp. Teor. Fiz.*, **20**, 1064.

Gregers-Hansen, P. E. and Levinsen, M. T. 1971, *Phys. Rev. Lett.*, **27**, 847.

Grimes, C. C., Richards, P. L. and Shapiro, S. 1968, *J. Appl. Phys.*, **39**, 3905.

Ivanchenko, Yu. M. and Zil'berman, L. A. 1969, *Sov. Phys. JETP*, **28**, 1272.

Josephson, B. D. 1965, *Adv. Phys.*, **14**, 419.

Josephson, B. D. 1962, *Phys. Lett.*, **1**, 251.

Kamper, R. A. and Zimmerman, J. E. 1971, *J. Appl. Phys.*, **42**, 132.

McCumber, D. E. 1968, *J. Appl. Phys.*, **39**, 2503.

McCarthy, S. L. and Warman, J. 1974, *J. Appl. Phys.*, to be published.

Richards, P. L. and Sterling, S. A. 1969 *Appl. Phys. Lett.*, **14**, 394.

Shapiro, S., Janus, A. R. and Holly, S. 1964, *Rev. Mod. Phys.*, **36**, 223.

Shapiro, S. 1963, *Phys. Rev. Lett.*, **11**, 80.

Song, Y. 1972, private communication.

Stephen, M. J. 1969, *Phys. Rev.*, **182**, 131.

Stewart, W. C. 1968, *Appl. Phys. Lett.*, **12**, 277.

Ulrich, B. T. 1974, *Rev. de Physique Appl.*, **9**, 111.

Waldram, J. R., Pippard, A. B. and Clarke, J. 1970. *Phil. Trans. Rev. Soc. (London)*, **268**, 265.

Warman, J. and Blackburn, J. A. 1971, *Appl. Phys. Lett.*, **19**, 60.

Warman, J., Jahn, M. T. and Kao, Y. H. 1971, *J. Appl. Phys.*, **42**, 5914.

Warman, J. 1972, PhD. Thesis. S.U.N.Y. at Stony Brook.

Wyatt, A. F. G. and Evans, D. H. 1969 in *Proc of Int. Conf. on the Science of Superconductivity,* (Stanford) p. 288.

Revista Mexicana de Astronomía y Astrofísica, Volumen 1, Abril 1974.

MULTICOLOR PHOTOMETRY OF METALLIC-LINE STARS I.

ν^1 DRACONIS AND ν^2 DRACONIS

EUGENIO E. MENDOZA V.

and

SALVADOR F. GONZÁLEZ *B.*
Instituto de Astronomía
Universidad Nacional Autónoma de México

Received 1974 February 28

RESUMEN

En este trabajo se describen observaciones fotométricas en el sistema UBVRI de BS6554 (ν^1 Dra) y BS6555 (ν^2 Dra). Actualmente se acepta que BS6555 es una estrella de la clase "metálica", Am. Pero hay discrepancia si BS6554 pertenece a este grupo espectroscópico o no. La fotometría que se obtuvo en el Observatorio Astronómico Nacional en San Pedro Mártir, B. C., indica que ambas estrellas, probablemente, son variables. La amplitud de la variabilidad es pequeña, del orden de un décimo de magnitud. A primera apreciación la variación parece irregular.

ABSTRACT

This paper describes UBVRI-photometric observations of the double star BS6554 (ν^1 Dra) and BS6555 (ν^2 Dra). Today, it is accepted that BS6555 is a metallic-line star, Am; however, there is not a general agreement as to whether BS6554 is an Am Star or not. The photometry indicates that probably both are variable stars. The variability amplitude is around 0.1 mag. At the first galance, the variables are irregular.

Key words: METALLIC LINE STARS—VARIABLE STARS—PHOTOMETRY.

I. INTRODUCTION

Titus and Morgan (1940) introduced the term "metallic-line star" (Am) for those stars, in the range A-F, which showed spectroscopic anomalies, namely, three different spectral types: one, from the K-line of CaII (the earliest), another, from hydrogen lines (intermediate) and the other, from the metallic-lines (the latest). The definition of classical metallic-line stars is based on only superficial spectroscopic features. However, the classification today is more subtle, involving narrow-band photometry or high dispersion spectra for its application. See, for instance Conti (1970).

Breger (1970) has suggested that pulsation and metallic-line phenomena are mutually exclusive in Am stars. Besell and Eggen (1972) have supplied an example of a pulsating metallic-line star, BS5491. However, Breger *et al.* (1972) found no evidence that BS5491 suffers light variation.

We were engaged in erecting and testing two telescopes at San Pedro Mártir Observatory in 1971. We observed BS6554 (ν^1 Dra) and BS6555 (ν^2 Dra) during this period.

This pair has been classified as Am by several astronomers (cf. Jaschek *et al.* 1964). Slettebak (1955) also gives the K-and metallic-line-types, A4 and A7 for BS6554 and A2 and F2 for BS6555. More recently, Cowley *et al.* (1969) classify BS6554 as an A6 V and BS6555 as an A4m. This indicates that, at least, ν^2 Draconis is a metallic-line star.

In the following sections we describe the observations, analyse the quality of the data and present the conclusions.

TABLE 1

STANDARD STARS

BS	MK	V	U−V	B−V	V−R	V−I	n
4456	B3 V	5.95	−0.81	−0.15	−0.10	−0.20	8
4550	G8 Vp	6.45	0.90	0.73	0.63	1.09	9
6603	K2 III	2.77	2.43	1.18	0.81	1.38	44
6629	A0 V	3.74	0.07	0.05	0.04	0.03	40
8622	09 V	4.89	−1.24	−0.21	−0.08	−0.30	21
8832	K3 V	5.59	1.86	0.99	0.84	1.37	20

TABLE 2

OBSERVED ATMOSPHERIC EXTINCTION

Filter Band	$\lambda_o(\mu)$	k		
		Tonantzintla	Tololo	S. Pedro M.
U	0.36	0.568		0.476
B	0.44	0.322	0.240	0.218
V	0.55	0.216	0.143	0.138
R	0.70	0.157	0.089	0.090
I	0.90	0.118	0.060	0.055
Months		Nov-Feb	Nov-Dec	June
Years		1963-4	1969	1971
nights		31	20	12

TABLE 3

PROBABLE ERROR OF A SINGLE OBSERVATION AT 1.0 AIR MASS

V	B−V	U−B	V−R	R−I
±0.015	±0.015	±0.019	±0.020	±0.018

II. THE OBSERVATIONS

The binary system BS6554 and BS6555 is well suited for accurate photometry because both stars are separated only by 62 seconds of arc and they also have similar colors. Under these conditions, the atmospheric extinction corrections are minimal, provided at least, one of them is a non variable star and the photo-electric equipment is stable.

We have made UBVRI photometry of ν^1 and ν^2 Dra at San Pedro Mártir Observatory in June 1971. Table 1 contains the standard stars observed in this program. The columns of this table give: first, the Bright Star (BS) Catalogue number (Hoffleit 1964); second, the MK type; third through seventh, the observed V magnitude and the observed U-V, B-V, V-R and V-I color indices, respectively; last, the number of independent observations.

The extinction coefficients were derived by the procedure outlined by Mendoza (1970). Table 2 lists the mean k-coefficient for U, B, V, R, and I for Tonantzintla, Tololo, and San Pedro Mártir Observatories. Table 3 contains the probable error of a single observation at 1.0 air mass for the measurements reported in this paper.

TABLE 4a

JOURNAL OF OBSERVATIONS OF BS6554

V	U−V	B−V	V−R	V−I	J.D. 2441100+
4.9	0.309	0.36	0.266	0.364	5.6784
4.902	0.319	0.235	0.235	0.343	5.7025
4.891	0.276	0.316	0.231	0.338	5.743
4.897	0.35	0.385	0.243	0.355	5.7602
4.88	0.313	0.335	0.216	0.323	5.8081
4.891	0.303	0.25	0.228	0.343	5.8236
4.89	0.288	0.227	0.216	0.334	5.8377
4.89	0.256	0.233	0.229	0.35	5.8516
4.897	0.268	0.228	0.237	0.349	5.8655
4.902	0.266	0.23	0.209	0.337	5.9268
4.932	0.327	0.248	0.24	0.369	5.944
4.898	0.323	0.283	0.239	0.344	5.9658
4.941	0.239	0.251	0.286	0.408	7.666
4.902	0.257	0.247	0.236	0.369	7.6827
4.87	0.265	0.259	0.22	0.341	7.717
4.896	0.277	0.241	0.243	0.381	7.7308
4.897	0.278	0.241	0.247	0.381	7.7455
4.874	0.267	0.244	0.218	0.342	7.7956
4.876	0.247	0.255	0.235	0.359	7.809
4.866	0.27	0.291	0.205	0.343	7.8227
4.849	0.271	0.274	0.216	0.331	7.8366
4.968	0.266	0.164	0.283	0.404	7.8928
4.951	0.284	0.281	0.265	0.385	7.9099
4.943	0.297	0.246	0.296	0.385	7.9504
4.887	0.271	0.253	0.232	0.34	10.6587
4.889	0.258	0.247	0.235	0.37	10.673
4.901	0.27	0.252	0.249	0.388	10.7059
4.907	0.258	0.248	0.246	0.388	10.7195
4.897	0.255	0.239	0.227	0.368	10.7339
4.897	0.255	0.204	0.243	0.392	10.7705
4.883	0.247	0.246	0.244	0.382	10.7859
4.901	0.251	0.243	0.26	0.409	10.8027
4.885	0.26	0.226	0.223	0.355	10.8194
4.875	0.243	0.236	0.241	0.383	10.842
4.864	0.282	0.267	0.244	0.364	11.7575
4.872	0.26	0.237	0.251	0.363	11.7719
4.898	0.275	0.254	0.271	0.375	11.7856
4.877	0.262	0.251	0.25	0.359	11.7993
4.917	0.279	0.25	0.281	0.405	11.8122
4.921	0.278	0.255	0.279	0.407	11.8276
4.948	0.289	0.252	0.286	0.404	11.8623
4.987	0.306	0.256	0.32	0.434	11.9063
4.98	0.252	0.259	0.319	0.455	11.9223
4.958	0.311	0.247	0.289	0.455	11.9614
4.971	0.277	0.236	0.385	0.521	11.9768
4.93	0.208	0.243	0.237	0.415	12.7179
4.883	0.171	0.249	0.239	0.421	12.765
4.897	0.17	0.258	0.262	0.443	12.7962
4.866	0.179	0.264	0.242	0.426	12.8102
4.883	0.18	0.27	0.23	0.415	12.8232

TABLE 4a—Continued

V	U−V	B−V	V−R	V−I	J.D. 2441100+
4.878	0.17	0.248	0.244	0.428	12.8364
4.85	0.252	0.251	0.186	0.318	15.8263
4.921	0.257	0.244	0.258	0.365	15.8687
4.94	0.261	0.267	0.264	0.389	15.8832
4.92	0.284	0.287	0.22	0.371	15.9072
4.97	0.25	0.203	0.315	0.432	15.9347
4.934	0.249	0.219	0.278	0.401	15.9606
4.935	0.268	0.248	0.271	0.391	15.9814
4.914	0.244	0.263	0.259	0.381	17.6981
4.876	0.247	0.252	0.213	0.335	17.7115
4.892	0.249	0.243	0.231	0.35	17.7245
4.887	0.272	0.264	0.228	0.366	17.7554
4.866	0.231	0.234	0.22	0.343	17.7684
4.869	0.236	0.265	0.207	0.325	17.7812
4.874	0.239	0.242	0.232	0.355	17.7939
4.872	0.237	0.258	0.226	0.348	17.8068
4.87	0.223	0.249	0.231	0.353	17.8212
4.939	0.265	0.216	0.257	0.38	17.8826
4.927	0.246	0.229	0.254	0.379	17.8991
4.914	0.246	0.228	0.243	0.379	17.9257
4.956	0.252	0.233	0.268	0.403	17.9505
4.94	0.269	0.238	0.26	0.388	17.9829
4.937	0.286	0.244	0.259	0.396	17.9975
4.892	0.269	0.223	0.245	0.342	19.7105
4.841	0.237	0.25	0.22	0.342	19.7444
4.88	0.231	0.197	0.231	0.374	19.7583
4.915	0.209	0.19	0.247	0.386	19.8274
4.915	0.197	0.203	0.219	0.383	19.8813
4.995	0.255	0.226	0.283	0.414	19.9154
4.911	0.252	0.261	0.253	0.374	21.7089
4.896	0.249	0.277	0.236	0.361	21.7403
4.887	0.257	0.265	0.243	0.373	21.7543
4.894	0.256	0.273	0.244	0.374	21.7673
4.883	0.248	0.258	0.267	0.371	21.7825
4.877	0.249	0.266	0.228	0.35	21.7969
4.872	0.252	0.272	0.239	0.369	21.812
4.922	0.246	0.27	0.267	0.404	21.8847
4.902	0.264	0.263	0.205	0.35	21.9002
4.897	0.218	0.239	0.235	0.397	21.9255
4.941	0.266	0.252	0.284	0.414	21.9513
4.929	0.22	0.224	0.246	0.396	21.9843
4.954	0.284	0.245	0.24	0.362	23.6945
4.91	0.268	0.248	0.253	0.382	23.7478
4.919	0.258	0.243	0.233	0.38	23.7611
4.9	0.261	0.255	0.232	0.367	23.7834
4.885	0.262	0.244	0.233	0.338	23.8041
4.909	0.283	0.238	0.254	0.372	23.8713
4.927	0.229	0.218	0.263	0.398	23.8867
4.88	0.254	0.228	0.252	0.362	23.918
4.876	0.223	0.236	0.231	0.342	23.9444

TABLE 4a—Continued

V	U−V	B−V	V−R	V−I	J.D. 2441100+
4.893	0.243	0.233	0.274	0.396	23.9798
4.885	0.226	0.225	0.259	0.386	23.9934
4.911	0.272	0.294	0.249	0.367	28.7594
4.917	0.261	0.27	0.234	0.339	28.774
4.927	0.231	0.253	0.251	0.357	28.787
4.928	0.23	0.261	0.254	0.353	28.8263
4.916	0.247	0.251	0.226	0.327	28.8702
4.903	0.261	0.264	0.2	0.304	28.8847
4.914	0.265	0.204	0.213	0.321	28.9103
4.953	0.237	0.268	0.295	0.418	28.9424
4.934	0.232	0.156	0.244	0.378	28.9786
4.91	0.261	0.256	0.25	0.351	32.6892
4.912	0.247	0.269	0.307	0.405	32.7036
4.913	0.283	0.201	0.253	0.353	32.7388
4.927	0.28	0.258	0.256	0.359	32.7531
4.912	0.277	0.265	0.247	0.357	32.7672
4.916	0.269	0.257	0.244	0.365	32.7803
4.93	0.276	0.222	0.306	0.429	32.8444
4.907	0..28	0.223	0.211	0.322	32.8579
4.914	0.291	0.238	0.218	0.367	32.8719
4.917	0.269	0.244	0.237	0.389	32.8843
4.916	0.276	0.248	0.23	0.374	32.897
4.922	0.292	0.258	0.259	0.391	32.9643

The journal of observations of BS6554 and BS6555 is listed in Tables 4a and 4b, respectively. The columns of these tables contain: first through fifth, the V magnitude, the U-V, B-V, V-R and V-I color indices, respectively; and last, the Julian Day.

III. THE QUALITY OF DATA

The photometric data for the standard stars (see Table 1), on the average, depart from the standard values (Johnson *et al.* 1966) ±0.01 mag. The probable errors quoted in Table 3 are approximately 20% larger than previous determinations (Mendoza 1967, 1970). However, the quality of the sky for photometry is excellent as indicated by the values of the extinction coefficients obtained in this observational period (cf. Table 2). Altogether, this indicates that the photometric measurements contained in Table 4 are reasonably good. Perhaps a slight instability of the photo-electric equipment was present.

TABLE 4b

JOURNAL OF OBSERVATIONS OF BS6555

V	U−V	B−V	V−R	V−I	J.D. 2441100+
4.873	0.397	0.318	0.254	0.346	5.6941
4.857	0.423	0.423	0.231	0.346	5.7105
4.872	0.385	0.304	0.242	0.343	5.7508
4.888	0.393	0.285	0.27	0.377	5.7681
4.851	0.386	0.305	0.211	0.348	5.8153
4.858	0.396	0.274	0.229	0.332	5.8311
4.856	0.371	0.281	0.267	0.365	5.8446
4.856	0.373	0.284	0.245	0.36	5.8586
4.864	0.364	0.272	0.239	0.361	5.8723
4.859	0.383	0.288	0.233	0.34	5.9352
4.914	0.357	0.266	0.218	0.409	5.9531
4.899	0.4	0.3	0.242	0.381	5.9738
4.893	0.351	0.3	0.262	0.393	7.674
4.893	0.335	0.257	0.283	0.417	7.6899
4.892	0.328	0.28	0.295	0.425	7.7238
4.887	0.327	0.283	0.272	0.41	7.7378
4.892	0.32	0.302	0.296	0.425	7.7531
4.851	0.315	0.315	0.262	0.398	7.8025
4.832	0.34	0.29	0.232	0.365	7.8159
4.839	0.333	0.294	0.242	0.371	7.8297
4.841	0.316	0.285	0.25	0.379	7.8443
4.926	0.359	0.3	0.284	0.425	7.9014
4.947	0.354	0.296	0.292	0.429	7.9177
4.927	0.359	0.334	0.292	0.434	7.9602
4.866	0.321	0.29	0.246	0.374	10.6656
4.877	0.313	0.231	0.248	0.397	10.68
4.881	0.336	0.278	0.259	0.405	10.7128
4.873	0.326	0.3	0.268	0.419	10.7265
4.882	0.311	0.249	0.271	0.428	10.7408
4.86	0.318	0.275	0.267	0.391	10.7775
4.859	0.328	0.25	0.249	0.408	10.7937
4.877	0.324	0.243	0.274	0.43	10.8103
4.886	0.313	0.219	0.273	0.433	10.8286
4.85	0.318	0.268	0.231	0.392	10.8496
4.868	0.331	0.286	0.286	0.415	11.7651
4.861	0.344	0.289	0.274	0.386	11.7791
4.869	0.34	0.286	0.288	0.408	11.7923
4.867	0.341	0.293	0.271	0.403	11.8056
4.858	0.365	0.315	0.267	0.392	11.82
4.869	0.364	0.272	0.254	0.383	11.8352
4.925	0.376	0.324	0.305	0.427	11.8703
4.952	0.372	0.288	0.319	0.449	11.9144
4.933	0.401	0.303	0.446	0.585	11.9316
4.947	0.355	0.265	0.311	0.472	11.9687
4.942	0.351	0.279	0.337	0.472	11.9851
4.93	0.242	0.265	0.281	0.279	12.7252
4.855	0.243	0.281	0.334	0.519	12.7718
4.849	0.247	0.299	0.245	0.453	12.8037
4.857	0.243	0.291	0.254	0.434	12.8167
4.852	0.252	0.284	0.259	0.442	12.8298

TABLE 4b—Continued

V	U−V	B−V	V−R	V−I	J.D. 2441100+
4.855	0.239	0.295	0.257	0.414	12.8428
4.846	0.311	0.284	0.229	0.355	15.8337
4.916	0.294	0.267	0.297	0.415	15.8759
4.919	0.294	0.262	0.292	0.407	15.8907
4.911	0.349	0.268	0.256	0.386	15.9137
4.915	0.355	0.293	0.383	0.518	15.9419
4.898	0.341	0.292	0.279	0.398	15.9728
4.883	0.372	0.315	0.294	0.41	15.9885
4.858	0.322	0.3	0.229	0.355	17.7047
4.872	0.315	0.241	0.269	0.395	17.7182
4.871	0.294	0.276	0.258	0.395	17.7307
4.858	0.302	0.29	0.249	0.382	17.7618
4.848	0.3	0.256	0.24	0.368	17.7749
4.86	0.309	0.275	0.257	0.388	17.7875
4.856	0.31	0.294	0.261	0.395	17.8001
4.841	0.308	0.29	0.254	0.38	17.8143
4.836	0.305	0.289	0.23	0.359	17.8281
4.918	0.292	0.201	0.281	0.421	17.8891
4.912	0.282	0.209	0.264	0.41	17.9084
4.899	0.296	0.242	0.271	0.401	17.9325
4.926	0.349	0.265	0.298	0.426	17.9577
4.911	0.353	0.252	0.285	0.417	17.9908
4.906	0.362	0.283	0.262	0.41	18.0043
4.869	0.349	0.268	0.255	0.384	19.7181
4.839	0.322	0.275	0.229	0.351	19.7517
4.886	0.341	0.289	0.172	0.386	19.7881
4.872	0.321	0.265	0.257	0.401	19.8344
4.911	0.34	0.259	0.216	0.423	19.8927
4.875	0.348	0.308	0.253	0.382	21.7156
4.871	0.325	0.27	0.258	0.379	21.7471
4.873	0.319	0.307	0.276	0.408	21.7608
4.857	0.32	0.302	0.258	0.383	21.7754
4.861	0.321	0.303	0.303	0.434	21.7902
4.855	0.328	0.31	0.254	0.375	21.8049
4.852	0.312	0.299	0.249	0.385	21.8192

TABLE 4b—Continued

V	U−V	B−V	V−R	V−I	J.D. 2441100+
4.882	0.326	0.288	0.253	0.386	21.8921
4.871	0.32	0.29	0.239	0.38	21.9081
4.881	0.328	0.283	0.273	0.409	21.9322
4.913	0.314	0.289	0.288	0.431	21.9582
4.908	0.292	0.284	0.275	0.402	21.9925
4.933	0.344	0.282	0.284	0.423	23.7025
4.888	0.337	0.29	0.273	0.411	23.7542
4.88	0.342	0.288	0.252	0.395	23.7694
4.875	0.32	0.271	0.271	0.411	23.7974
4.852	0.343	0.295	0.252	0.387	23.8107
4.896	0.31	0.247	0.287	0.42	23.8784
4.892	0.346	0.263	0.271	0.432	23.8936
4.841	0.321	0.298	0.256	0.367	23.9273
4.849	0.3	0.276	0.266	0.401	23.9513
4.862	0.313	0.265	0.294	0.384	23.987
4.889	0.335	0.308	0.271	0.378	28.7672
4.892	0.314	0.305	0.269	0.361	28.7805
4.888	0.313	0.304	0.261	0.375	28.7971
4.884	0.297	0.29	0.242	0.371	28.8325
4.88	0.31	0.275	0.215	0.337	28.8767
4.894	0.324	0.285	0.239	0.367	28.8924
4.91	0.279	0.282	0.241	0.354	28.9182
4.911	0.337	0.307	0.233	0.357	28.9498
4.894	0.314	0.281	0.32	0.425	32.6968
4.895	0.326	0.279	0.283	0.389	32.7112
4.897	0.332	0.288	0.273	0.382	32.7456
4.892	0.394	0.302	0.263	0.389	32.7597
4.894	0.355	0.293	0.268	0.388	32.7737
4.891	0.342	0.281	0.255	0.37	32.7865
4.89	0.358	0.284	0.244	0.371	32.8511
4.902	0.345	0.269	0.265	0.393	32.8654
4.887	0.352	0.275	0.254	0.381	32.8782
4.888	0.358	0.279	0.262	0.403	32.8906
4.893	0.348	0.283	0.263	0.395	32.9039
4.902	0.355	0.279	0.33	0.449	32.9704

A simple statistical analysis of the observations gives the standard deviations for both the standard and program stars. The values are contained in Table 5. These quantities for BS6554 and BS6555 are, on the average, 1.3 times larger than those of the standard stars. This can also be shown in the plots of the magnitude (or colors) *versus* Julian Day (González 1974). In addition, these graphs, as well as Table 4, indicate amplitudes of the variations of around 0.1 mag.

It should be pointed out that values obtained from differences of magnitude and colors of ν^1 and ν^2 Draconis show scatter similar to the original observations. This is shown in Tables 5 (last row) and 6. Graphs derived from Tables 4 and 6 will be given by González (1974).

IV. CONCLUSION

We have presented UBVRI-photometry of the double star BS6554-5. At least one of the components is an Am (BS6555). The observational data given above, indicate that probably both stars show small light variation of approximately 0.1 mag. Perhaps BS6554 has a larger amplitude than BS6555 by a few hundredths of a magnitudes.

An indication of the variability in V and B-V of this binary is found in the literature (Blanco *et al.*

TABLE 5

STANDARD DEVIATIONS

BS	σ(V)	σ(B−V)	σ(U−B)	σ(V−R)	σ(R−I)	n
			Standard Stars			
4456	0.014	0.021	0.016	0.032	0.026	8
4550	0.017	0.026	0.030	0.024	0.019	9
6603	0.019	0.022	0.025	0.023	0.018	44
6629	0.023	0.018	0.028	0.021	0.021	40
8622	0.019	0.020	0.029	0.023	0.015	21
8832	0.020	0.024	0.022	0.021	0.013	20
			ν^1 Dra and ν^2 Dra			
6554	0.029	0.029	0.035	0.028	0.019	123
6555	0.027	0.025	0.034	0.032	0.025	120
Δ	0.023	0.032	0.029	0.027	0.027	190

Note to Table 5:
Δ = BS6555 − BS6554

TABLE 6

DIFFERENCES BETWEEN BS 6555 AND BS 6554

ΔV	ΔB−V	ΔU−B	ΔV−R	ΔR−I	J.D. 2441100+
-0.027	-0.043	0.130	-0.012	-0.006	5.6862
-0.029	0.083	-0.005	0.019	-0.016	5.6983
-0.045	0.188	-0.084	-0.004	0.007	5.7065
-0.019	-0.012	0.121	0.011	-0.006	5.7469
-0.025	-0.081	0.116	-0.001	-0.011	5.7555
-0.009	-0.100	0.143	0.027	-0.005	5.7641
-0.029	-0.030	0.103	-0.005	0.030	5.8117
-0.040	0.055	0.028	-0.017	0.022	5.8194
-0.033	0.024	0.069	0.001	-0.012	5.8273
-0.032	0.047	0.061	0.013	-0.015	5.8344
-0.034	0.054	0.029	0.051	-0.020	5.8411
-0.034	0.048	0.067	0.038	-0.023	5.8481
-0.034	0.051	0.066	0.016	-0.006	5.8551
-0.041	0.056	0.049	0.008	0.003	5.8620
-0.033	0.044	0.052	0.002	0.010	5.8689
-0.043	0.058	0.059	0.024	-0.021	5.9310
-0.073	0.040	0.016	-0.007	-0.022	5.9386
-0.018	0.018	0.012	-0.022	0.062	5.9485
0.016	-0.017	0.051	-0.021	0.086	5.9594
0.001	0.017	0.060	0.003	0.034	5.9698
-0.048	0.049	0.063	-0.024	0.009	7.6700
-0.009	0.053	0.041	0.026	-0.002	7.6783
-0.009	0.010	0.068	0.047	0.001	7.6863
0.022	0.021	0.042	0.075	0.009	7.7204
-0.004	0.039	0.012	0.052	-0.008	7.7273
-0.009	0.042	0.012	0.029	0.000	7.7343
-0.010	0.042	0.007	0.025	0.004	7.7416
-0.005	0.061	-0.019	0.049	-0.005	7.7493
-0.023	0.071	-0.023	0.044	0.012	7.7990
-0.025	0.060	0.008	0.027	0.012	7.8057
-0.044	0.035	0.058	-0.003	0.009	7.8124
-0.034	-0.001	0.071	0.027	-0.005	7.8193
-0.027	0.003	0.060	0.037	-0.009	7.8262

TABLE 6 — Continued

ΔV	ΔB−V	ΔU−B	ΔV−R	ΔR−I	J.D. 2441100+
-0.010	0.020	0.042	0.026	0.014	7.8331
-0.008	0.011	0.034	0.034	0.014	7.8404
-0.042	0.136	-0.043	0.001	0.020	7.8971
-0.025	0.019	0.056	0.019	0.021	7.9056
-0.004	0.015	0.055	0.027	0.017	7.9138
-0.016	0.088	-0.026	-0.004	0.053	7.9553
-0.021	0.037	0.013	0.014	0.020	10.6621
-0.023	0.043	0.020	0.011	-0.007	10.6693
-0.012	-0.016	0.071	0.013	0.014	10.6765
-0.020	0.026	0.040	0.010	0.007	10.7093
-0.026	0.030	0.048	0.013	0.004	10.7161
-0.034	0.052	0.016	0.022	0.009	10.7230
-0.024	0.061	0.010	0.041	0.010	10.7302
-0.015	-0.010	-0.046	-0.044	0.016	10.7373
-0.037	0.071	-0.008	0.024	-0.025	10.7740
-0.023	0.029	0.042	0.023	-0.014	10.7817
-0.024	0.004	0.077	0.005	0.021	10.7898
-0.042	0.007	0.070	-0.011	0.010	10.7982
-0.024	0.000	0.073	0.014	0.007	10.8065
-0.008	0.017	0.047	0.051	0.024	10.8148
0.001	-0.007	0.060	0.050	0.028	10.8240
0.011	-0.017	0.087	0.032	0.018	10.8353
-0.025	0.032	0.043	-0.010	0.019	10.8458
0.004	0.019	0.030	0.042	0.009	11.7613
-0.004	0.049	0.022	0.035	0.017	11.7685
-0.011	0.052	0.032	0.023	0.000	11.7755
-0.037	0.035	0.034	0.003	0.008	11.7823
-0.029	0.032	0.033	0.017	0.016	11.7889
-0.008	0.035	0.043	0.038	0.011	11.7958
-0.010	0.042	0.037	0.021	0.023	11.8024
-0.050	0.043	0.019	-0.010	0.008	11.8089
-0.059	0.065	0.021	-0.014	0.001	11.8161
-0.063	0.060	0.027	-0.012	-0.003	11.8238
-0.052	0.017	0.069	-0.025	0.001	11.8314
-0.023	0.072	0.015	0.019	0.004	11.8663

TABLE 6 — Continued

ΔV	ΔB−V	ΔU−B	ΔV−R	ΔR−I	J.D. 2441100+
-0.035	0.032	0.034	-0.001	0.016	11.9103
-0.028	0.029	0.091	0.000	-0.006	11.9183
-0.047	0.044	0.105	0.127	0.003	11.9269
-0.011	0.018	0.026	0.022	-0.005	11.9650
-0.024	0.029	0.049	-0.074	0.025	11.9727
-0.029	0.043	0.031	-0.048	-0.001	11.9809
0.000	0.022	0.012	0.044	-0.180	12.7215
0.047	0.016	0.055	0.042	-0.184	12.7451
-0.028	0.032	0.040	0.095	0.003	12.7684
-0.048	0.041	0.036	-0.017	0.027	12.7999
-0.017	0.035	0.033	0.003	0.024	12.8069
-0.009	0.027	0.037	0.012	-0.004	12.8134
-0.026	0.021	0.042	0.024	-0.005	12.8199
-0.031	0.014	0.058	0.029	-0.002	12.8265
-0.026	0.036	0.046	0.015	-0.001	12.8331
-0.023	0.047	0.022	0.013	-0.027	12.8396
-0.004	0.033	0.026	0.043	-0.006	15.8300
-0.005	0.023	0.014	0.039	0.011	15.8723
-0.024	0.000	0.033	0.033	-0.007	15.8795
-0.021	-0.005	0.038	0.028	-0.010	15.8869
-0.009	-0.019	0.084	0.036	-0.021	15.9104
-0.055	0.090	0.015	0.068	0.018	15.9383
-0.036	0.073	0.019	0.001	-0.004	15.9667
-0.037	0.044	0.029	0.008	-0.001	15.9771
-0.052	0.067	0.037	0.023	-0.004	15.9849
-0.056	0.037	0.041	-0.030	0.004	17.7014
-0.018	0.048	0.027	0.016	0.004	17.7081
-0.004	-0.011	0.079	0.056	0.004	17.7148
-0.020	-0.002	0.068	0.037	0.007	17.7213
-0.021	0.033	0.012	0.027	0.018	17.7276
-0.029	0.026	0.004	0.021	-0.005	17.7586
-0.008	0.056	0.015	0.029	0.010	17.7651
-0.018	0.022	0.047	0.020	0.005	17.7716
-0.021	-0.009	0.073	0.033	0.010	17.7781
-0.009	0.010	0.063	0.050	0.013	17.7843
-0.014	0.033	0.037	0.025	0.008	17.7907
-0.018	0.052	0.018	0.029	0.011	17.7970
-0.016	0.036	0.037	0.035	0.012	17.8034
-0.031	0.032	0.039	0.028	0.004	17.8105
-0.029	0.041	0.044	0.023	0.004	17.8177
-0.034	0.040	0.042	-0.001	0.007	17.8245
-0.021	-0.015	0.042	0.024	0.017	17.8858
-0.009	-0.028	0.074	0.027	0.015	17.8941
-0.015	-0.020	0.056	0.010	0.021	17.9037
-0.015	0.014	0.036	0.028	-0.006	17.9291
-0.030	0.032	0.065	0.030	-0.007	17.9541
-0.029	0.014	0.070	0.025	0.004	17.9868
-0.026	0.008	0.059	0.026	-0.005	17.9941
-0.031	0.039	0.037	0.003	0.011	18.0009
-0.023	0.045	0.035	0.010	0.032	19.7143
-0.002	0.025	0.060	0.009	0.000	19.7480
-0.041	0.078	0.013	-0.002	-0.021	19.7550
0.006	0.092	0.018	-0.059	0.071	19.7732
-0.029	0.099	0.033	-0.075	0.075	19.8077
-0.043	0.075	0.037	0.010	0.005	19.8309
-0.004	0.056	0.087	-0.003	0.043	19.8870
-0.084	0.032	0.052	0.067	0.076	19.9040
-0.036	0.047	0.049	0.000	0.008	21.7122
-0.025	-0.007	0.083	0.022	-0.004	21.7437
-0.016	0.005	0.063	0.015	-0.009	21.7507
-0.014	0.042	0.020	0.033	0.002	21.7575

TABLE 6 — Continued

ΔV	ΔB−V	ΔU−B	ΔV−R	ΔR−I	J.D. 2441100+
-0.021	0.034	0.029	0.032	0.002	21.7640
-0.037	0.029	0.035	0.014	-0.005	21.7713
-0.026	0.044	0.028	0.009	0.021	21.7789
-0.022	0.045	0.028	0.036	0.027	21.7863
-0.016	0.037	0.035	0.075	0.009	21.7935
-0.022	0.044	0.035	0.026	-0.001	21.8009
-0.017	0.038	0.038	0.014	-0.009	21.8084
-0.020	0.027	0.033	0.010	0.006	21.8156
-0.040	0.018	0.062	-0.014	-0.004	21.8884
-0.020	0.025	0.037	0.048	-0.012	21.8961
-0.031	0.027	0.029	0.034	-0.004	21.9041
-0.016	0.044	0.066	0.038	-0.026	21.9288
-0.028	0.037	0.011	0.004	0.013	21.9547
-0.021	0.060	0.012	0.029	-0.023	21.9884
-0.021	0.037	0.023	0.044	0.009	23.6985
-0.022	0.042	0.027	0.020	0.009	23.7510
-0.031	0.047	0.032	0.040	-0.009	23.7576
-0.039	0.045	0.039	0.019	-0.004	23.7652
-0.020	0.033	0.048	0.020	0.008	23.7764
-0.025	0.016	0.043	0.039	0.005	23.7904
-0.010	0.027	0.031	0.038	0.035	23.8007
-0.033	0.051	0.030	0.019	0.030	23.8074
-0.013	0.009	0.018	0.033	0.015	23.8748
-0.031	0.029	0.052	0.024	-0.002	23.8825
-0.035	0.045	0.072	0.008	0.026	23.8901
-0.039	0.070	-0.003	0.004	0.001	23.9226
-0.027	0.040	0.037	0.035	0.024	23.9478
-0.031	0.032	0.038	0.020	-0.032	23.9834
-0.023	0.040	0.047	0.035	-0.037	23.9902
-0.022	0.014	0.049	0.022	-0.011	28.7633
-0.028	0.038	0.036	0.037	0.002	28.7706
-0.025	0.035	0.018	0.035	0.013	28.7772
-0.035	0.052	0.031	0.018	0.014	28.7837
-0.039	0.051	0.031	0.010	0.008	28.7920
-0.044	0.029	0.038	-0.012	0.030	28.8294
-0.036	0.024	0.039	-0.011	0.021	28.8734
-0.023	0.011	0.038	0.015	0.018	28.8807
-0.009	0.021	0.042	0.039	0.024	28.8885
0.004	0.078	-0.064	0.028	0.005	28.9142
-0.042	0.039	0.061	-0.062	0.001	28.9461
-0.023	0.151	0.045	-0.011	-0.010	28.9642
-0.016	0.025	0.028	0.070	0.004	32.6930
-0.018	0.012	0.055	0.013	0.007	32.7002
-0.017	0.010	0.069	-0.024	0.008	32.7074
-0.016	0.087	0.038	0.020	0.009	32.7422
-0.030	0.030	0.022	0.017	0.006	32.7493
-0.035	0.044	0.070	0.007	0.023	32.7564
-0.020	0.037	0.080	0.016	0.016	32.7634
-0.018	0.028	0.050	0.021	0.010	32.7704
-0.022	0.036	0.050	0.022	-0.001	32.7770
-0.025	0.024	0.049	0.011	0.006	32.7834
-0.040	0.062	0.020	-0.062	0.004	32.8477
-0.017	0.061	0.017	0.033	0.016	32.8545
-0.005	0.046	0.019	0.054	0.017	32.8616
-0.012	0.031	0.023	0.047	-0.021	32.8686
-0.027	0.037	0.024	0.036	-0.022	32.8750
-0.030	0.031	0.052	0.017	-0.025	32.8812
-0.029	0.035	0.054	0.025	-0.011	32.8874
-0.028	0.031	0.051	0.032	-0.003	32.8938
-0.023	0.035	0.037	0.033	-0.012	32.9504
-0.020	0.021	0.042	0.071	-0.013	32.9673

TABLE 7

CATALINA OBSERVATIONS

V	U−V	B−V	V−R	V−I	J.D. 2438000+
			BS6554		
4.896	0.335	0.289	0.260	0.442	152.9288
4.909	0.239	0.238	0.203	0.335	165.8982
4.925	0.239	0.259	0.225	0.341	183.8666
4.831	0.333	0.297	0.260	0.371	224.7539
			BS6555		
4.919	0.239	0.247	0.253	0.418	152.9365
4.879	—	0.278	0.240	0.364	165.9032
4.893	0.320	0.297	0.241	0.367	183.8725
4.914	0.250	0.233	0.230	0.326	203.7949
4.862	0.254	0.263	0.244	0.347	224.7603

1968; Jaschek *et al.* 1972). Catalina photometry (Johnson *et al.* 1966) includes BS6554 and BS6555. This data is reproduced in Table 7. Here also variability can be inferred.

TABLE 8

MEAN MAGNITUDE AND COLORS

BS	V	U−V	B−V	V−R	V−I
6554	4.91	0.26	0.25	0.25	0.37
6555	4.88	0.33	0.28	0.27	0.40

Finally Table 8 contains the mean values of BS6554 and BS6555 as derived from Table 4.

We intend to obtain more multicolor photometry of BS6554-5 and other Am stars in order to study the possible existence of multi-periods, and the nature of their light curves, if any. Those of ν^1 and ν^2 Dra, at the first glance look like irregular variables; perhaps a Fourier analysis will tell otherwise.

E. Mendoza is indebted to the IBM Latin American Scientific Center for providing computing facilities.

REFERENCES

Besell, M. A., and Eggen, O. J. 1972, *Pub. A.S.P.*, **84**, 72.
Blanco, V. M., Demers, S., Douglass, G. G., and Fitzgerald, M. P. 1968, *Publ. U.S.N.O.*, Volume 21, second series.
Breger, M. 1970, *Ap. J.*, **162**, 597.
Breger, M., Maitzen, H. M., and Cowley, A. P. 1972, *Pub. A.S.P.*, **84**, 443.
Conti, P. S. 1970, *Pub. A.S.P.*, **82**, 781.
Cowley, A., Cowley, Ch., Jaschek, M., and Jaschek, C. 1969, *A. J.*, **74**, 375.
González, S. F. 1974, *in preparation.*
Hoffleit, D. 1964, *Catalogue of Bright Stars* (New Haven, Conn.: Yale University Observatory).
Jaschek, C., Conde, H., and Sierra, A. 1964, *Obs. Astr. Univ. de la Plata,* Serie Astronómica **28** (2).
Jaschek, C., Hernández, E., Sierra A., and Gerhardt, A. 1972, *Obs. Astr. Univ. de la Plata,* Serie Astronómica **38**.
Johnson, H. L., Mitchell, R. I., Iriarte, B., and Wisniewski, W. Z. 1966, *Comm. Lunar & Planetary Lab.*, **4**, 99.
Mendoza, E. E. 1970, *Bol. Obs. Tonantzintla y Tacubaya,* **5**, 269.
Slettebak, A. 1955, *Ap. J.*, **121**, 653.
Titus, J., and Morgan, W. W. 1940, *Ap. J.*, 92, 256.

Revista Mexicana de Astronomía y Astrofísica, Volumen 1, Abril 1974.

A FOLDED SCHMIDT CAMERA FOR A TELEVISION MULTICHANNEL SENSOR

L. E. Celaya, F. Cobos and C. Firmani

Instituto de Astronomía
Universidad Nacional Autónoma de México
Received 1974 February 28

RESUMEN

Se propone el diseño óptico de una cámara Schmidt doblada f/2.9 para el acoplamiento entre un espectrógrafo Cassegrain de baja dispersión y un detector televisivo. La calidad de la imagen resulta mejor que el poder resolutivo del detector en el rango espectral comprendido entre 3000 Å y 11000 Å. La pérdida de luz debida a la obstrucción central es del orden del 15% y la inclinación del plano focal es despreciable.

ABSTRACT

An optical design of a folded Schmidt camera f/2.9, for coupling a low dispersion Cassegrain spectrograph and a TV-detector, is proposed. The image obtained is better than the detector's resolution power in the spectral range between 3000 Å and 11000 Å. The central obstruction introduces a light loss of about 15% and the focal plane tilt is negligible.
Key words: OPTICAL DESIGN—SPECTROSCOPY.

I. INTRODUCTION

A design of an optical device, for coupling a vidicon TV-tube with a low dispersion Cassegrain spectrograph, is proposed. The television detector is arranged as a 500 channel array analyser with a spectral sensitivity range between 3000 Å and 11000 Å. The sensitive zone on the face plate of the TV-tube has a length of 1.25 cm, which corresponds to a resolution power of 25 μm in the direction of the light dispersion, and a maximum height of 1 cm in the direction of the slit image. The sky light and the dark current are subtracted from each channel during the signal read-out. The dark current is also reduced by working the TV-tube at dry ice temperature. The focal ratio of the spectrograph is f/15 and its focal length is 110.5 cm.

These characteristics and the seeing limitation suggested the design of a camera with a focal ratio approximately f/2.9. In this way, the resolution and the efficiency are optimized by using the spectrograph with a slit width corresponding to 2 arcseconds. The dispersion for a 400 lines/mm grating is 2.8 Å/channel in the first diffraction order.

The wide spectral range introduces severe conditions on the design, but a flat-field Schmidt camera, with refractive elements of fused quartz (homosil) gives a good solution to this problem. Finally, a folded Schmidt camera, of the type described by Epps and Peters (1973) provides low light loss and good flexibility for the coupling with the TV-tube cooling device.

II. OPTICAL DESIGN

It is necessary to consider with care the input and output conditions that are imposed on the camera by the whole system. The input to the camera is defined by the pupil coming out from the spectro-

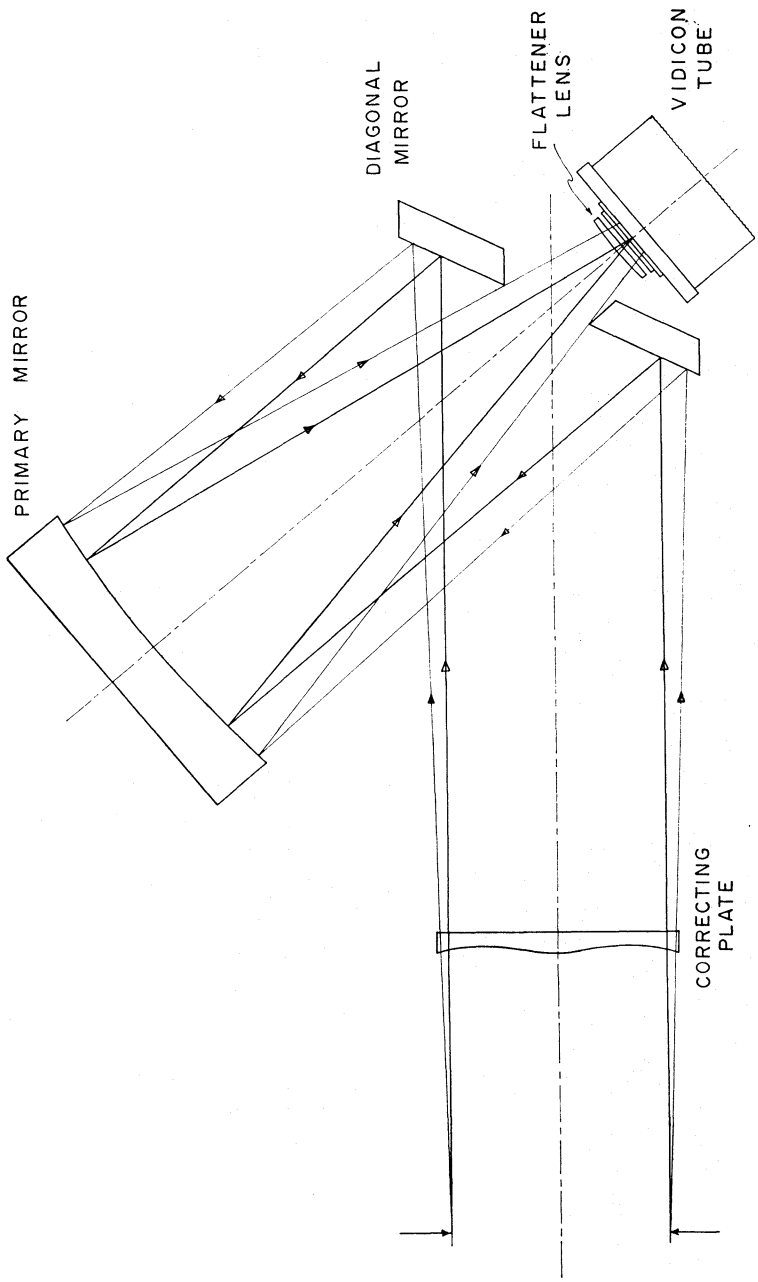

FIG. 1. Section drawing of the folded Schmidt camera f/2.9. The light dispersion is in the figure plane. Axial and marginal rays are shown.

Fig. 2. Spot diagram at different wavelengths for on-axis (below) and edge images (above). Focusing is optimized

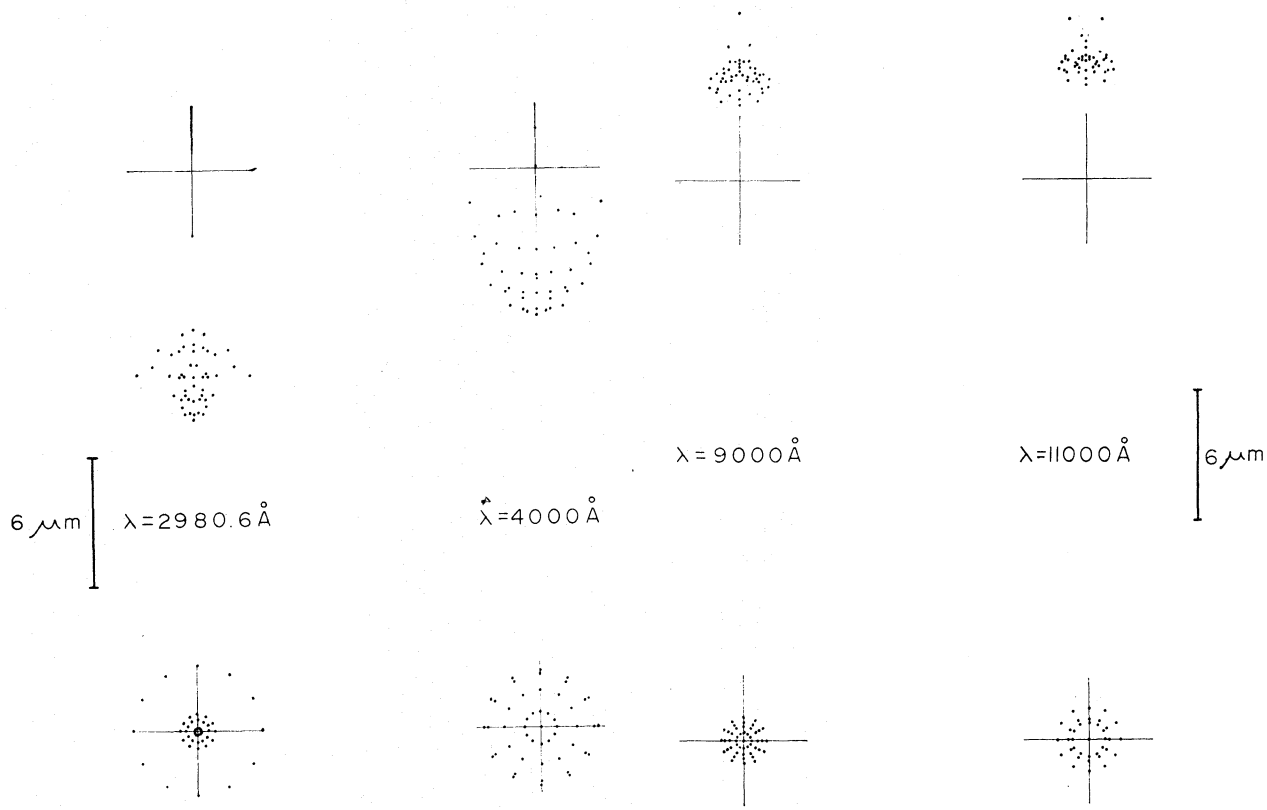

FIG. 3. Spot diagrams similar to Figure 2. Focus is optimized for ultraviolet light.

FIG. 4. Spot diagrams similar to Figure 2. Focus is optimized for infrared light.

graph grating. The distance between this pupil and the corrector plate was reduced, as far as mechanically possible, to minimize the optical aberrations. The camera output is conditioned by the TV-tube input feature: the vidicon has a quartz front face of 1.60 mm thickness and behind it is placed the silicon target at 1.23 mm; upon this target the image has to be focused. These factors have been considered in the optical design.

The camera optical features are presented in Tables 1 and 2 and the drawing of the camera is shown in Figure 1.

The central "obstruction", which is produced by the hole in the diagonal mirror, introduces a light loss of approximately 15%. The distance between the diagonal mirror and the TV-tube has been made as large as possible to obtain sufficient thermal isolation. The only optical element at dry ice temperature being the flattener field lens.

The on-axis image quality as well as the image quality at the edge of the field are shown in the spot diagrams of Figure 2 for different wavelengths. In these diagrams the focusing is optimized for blue light. It is evident that the image size is always smaller than 25 μm in all the spectral range considered; in this way, the resolution is limited by the TV-tube itself. The optical distortion is also maintained smaller than 25 μm. However, it is customary to work with limited portions of this spectral range (of the order of 1000 Å at a time). In this case,

TABLE 1

FINAL PARAMETERS OF THE LENS DESIGN

Radius of Curvature in cm	Thickness in cm	Glass
∞ *		
	9.525	Air
3124.57 **		
	0.7	Fused Quartz (Homosil)
∞		
	39.18	Air
−44.1876		
	−21.4644	Air
−9.8166		
	−0.28	Fused Quartz (Homosil)
31.9644		
	−0.11698	Air
∞ ***		
	−0.16002	Fused Quartz (Homosil)
∞		
		Air

* Pupil of the optical system.
** The aspheric constants of this surface are: $A_2 = -5.81 \times 10^{-6}$ and $A_3 = -1.29 \times 10^{-8}$.
*** Quartz plate of the vidicon TV-tube.

the camera can be focused at the desired color, thus it is possible to improve the image size, as shown in Figures 3 and 4.

As a final remark, it is interesting to note that the good image quality for a focus position, Figure 2, implies that the focal plane tilt is negligible. This makes the alignement of the TV-tube unnecessary with respect to the camera, each time that the observed spectral range is changed.

TABLE 2

FINAL CHARACTERISTICS OF THE LENS DESIGN

Design Characteristic	Final value	
Clear Aperture	7.4	cm
Focal Length	21.48	cm
Back Focal Length	0.123	cm
Correcting Plate Diameter	8.20	cm
Primary Mirror Clear Diameter	11.28	cm
Flattener Lens Clear Diameter	1.99	cm
Diagonal Mirror Thickness	1.10	cm
Focal Ratio	2.90	
Field Size	1.25	cm (3.33°)

The authors are indebted to J. de la Herrán for mechanical engineering advice and fruitful discussions. The drawings were prepared by V. Cajero.

REFERENCES

Epps, H. W. and Peters, P. J. 1973, *Proceedings of the Symposium "Astronomical Observations with Television Type Sensors"*, ed. J. W. Glaspey and G. A. H. Walker (Vancouver: Institute of Astronomy and Space Science, U. B. C.), p. 415.